

2D Dynamic Numerical Modelling of a Tunnel – Soil – Building System Subjected to Seismic Loading

Zhengyao He¹ and S. P. Gopal Madabhushi¹

¹Department of Engineering, University of Cambridge, UK

E-mail: za301@cam.ac.uk

ABSTRACT: It is important to determine dynamic tunnel behaviour under cyclic loading for the seismic underground structural design. The dynamic response of tunnels is further complicated when considering the interaction with surface buildings. This paper investigates a series of 2D plane-strain numerical models to study the dynamic response of a shallow cut-and-cover rectangular tunnel in loose, cohesionless soil. Both dry and saturated conditions are considered. Input motion includes sinusoidal waves with 10 cycles of shaking. A raft foundation with a 50 kPa structural surcharge is adopted to simulate the effect of the surface building. Soil displacements, wave propagation, earth pressures and tunnel lining structural response are determined. These results show that the soil liquefaction introduced by accumulated excess pore pressures causes the attenuation of soil horizontal acceleration, reduction of soil effective stresses and promotes tunnel flotation. The existence of a building not only reduces the liquefaction ratio of sub-surface soil right below the foundation but also effects the earth pressure distribution on the adjacent tunnel sidewall. In addition, the presence of the tunnel may affect adversely the rotation of the foundation especially in saturated soils.

KEYWORDS: Tunnel Flotation, Liquefaction, Cut & Cover Tunnel, and Soil-Structure Interaction (SSI).

1. INTRODUCTION

The development of underground tunnelling in urban areas has become more frequent, due to the growth of demand for space for utility, highway, and railway transportation in congested urban spaces. Shallow cut-and-cover tunnels are preferred in urban spaces as these are cheaper to build and technologically more straight forward to construct. Further, the cost of construction of a tunnel increases significantly with depth. However, these shallow tunnels can be close to the foundations of existing structures in an urban environment.

There is significant research directed towards the analyses of tunnels and tunnel construction processes. For example, Likitlersuang et al. (2014) analyzing the tunneling-induced surface settlement with hardening soil model. Phutthananon et al. (2023) utilized the same constitutive model to study the pile response due to adjacent tunnelling. Muenpetch et al. (2023) studied the influence zone of the twin tunnel excavation with hypoplastic model in PLAXIS 3D.

During a strong earthquake, there will be a strong interaction between the tunnel and the super-structure. For example, the tunnel linings may see additional loads due to the seismic loading that are enhanced by the presence of an adjacent structure. Recent seismic events, such as the Kobe earthquake in Japan, 1995, the Chi-chi earthquake in Taiwan, 1999, and the Wenchuan earthquake in China, 2008 indicated that underground structures have a high potential to be damaged by cyclic loads.

In the past decades, many researchers have focused their research on the understanding of the dynamic tunnel response subjected to the seismic load. A state-of-the-art paper published recently by Tsinidis et al. (2020) identifies the current understanding on the seismic behaviour of tunnels and the need for further research. Seismic loading on tunnels can lead to two major safety concerns, namely the soil-structure-interaction effects such as tunnel lining structural damages due to the seismic inertial forces, and in loose, saturated soils, the soil uplift or tunnel flotation due to the generated excess pore pressure below the tunnel invert. Seismic tunnel response was investigated using both physical modelling and numerical analyses. Cilingir and Madabhushi (2011a) studied square tunnel lining response and earth pressure with different tunnel lining flexibility with tunnels located in dry, loose sand. The circular tunnel response is also studied by Cilingir and Madabhushi (2011b, 2011c). However, it should be noted that most of the underground structures are not constructed in free field condition but located in congested urban areas in the proximity of other surface structures. It is necessary to

consider the variety of surcharge load distribution at the surface, such as different types of the building foundations, and the road pavement to simulate a more realistic scenario. Figure 1 shows an example of the tunnel-structures system, which is commonly observed in the urban area.

Tunnels are also vulnerable when located in loose, saturated soils due to the occurrence of soil liquefaction. Sukkarak et al. (2021) and Mase et al. (2022) provided valuable field data on assessing the liquefaction potential of the sandy soil at the North Thailand and Osaka Japan based on a series of site investigation and numerical approach. Tunnel flotation due to horizontal cyclic loads in saturated soil has been widely observed from the dynamic centrifuge testing by Chian and Madabhushi (2012), the 1-g shaking table testing by Watanabe et al. (2016), Taylor and Madabhushi (2020), and the 2D finite element analysis for rectangular tunnels by Madabhushi and Madabhushi (2015), and for circular tunnels by Chian et al. (2014). Chou et al. (2008a, 2008b, 2011) tested the uplift of a cut-and-cover tunnel in the BART Transbay Tube (TBT) project at California, using the centrifuge testing and considered a realistic geological soil profile. Seismic failure mechanism of the surface excavation in liquefiable soil has been numerically investigated by Petchkaew et al. (2023a, 2023b), and Hong-in et al. (2023). Pore pressures in the soil are cumulatively built up during the earthquake loading, causing a significant reduction in the shear strength of the soil, which is commonly defined as soil liquefaction. This flotation is even more serious when the tunnels are buried at shallow depth due to low vertical resistance against flotation. Early research on the shallow tunnel structures adjacent to existing surface buildings was carried out by Bilotta et al. (2017) as part of the SERA project.

Dynamic tunnel behaviour during the earthquake, such as the tunnel rocking and the tunnel uplift due to the soil liquefaction cause can cause significant safety risk to the tunnel and to the adjacent surface structures and buried utilities at shallow depth. This is particularly important for the underground construction in heavily populated urban areas, such as the recent George Massey Tunnel development in Vancouver, and the Shenzhen-Zhongshan Link at the Greater Bay area have all considered dynamic SSI during the seismic design.

This study presents the effect of surface structural loads such as the building on a shallow raft foundation, on the dynamic response of the rectangular tunnel and adjacent soil when subjected to lateral shaking at bedrock level to due to a seismic event. Soil moisture conditions are considered separately as fully dry or fully saturated. The aim of this research is to investigate, using numerical analyses,

the tunnel lining behaviour and building settlements for the dry case, and the soil excess pore pressures, the shear wave propagation through the sandy soil, as well as the surface movement during and after application of seismic loading for the saturated case.

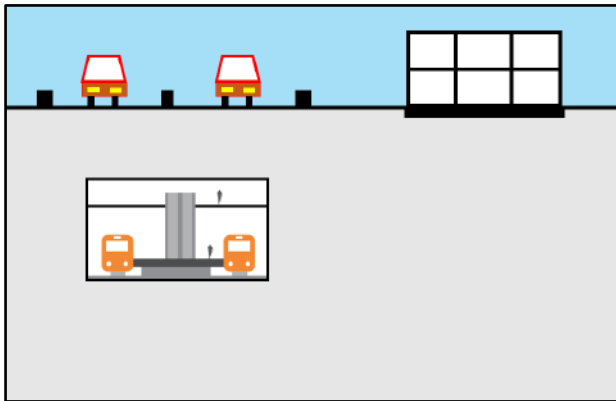


Figure 1 Typical geometry of the tunnel – structural interaction problem

2. NUMERICAL MODELLING

Numerical modelling based on finite element analyses in time domain has been proven as an effective tool to undertake complex geotechnical and SSI problems. The recent Round Robin Tunnel Test (RRTT) project compared the tunnel dynamic response obtained from the centrifuge data conducted by Lanzano et al. (2012), with numerical simulation results based on 5 different constitutive models (Bilotta et al., 2014). Research outputs confirmed the feasibility and acceptable accuracy of the finite element analysis in solving dynamic tunnel-soil system. The current study presents the numerical analyses carried out using a 2D generalised plasticity based finite element code SWANDYNE under plane strain assumption, developed by Chan (1988). SWANDYNE is an effective stress-based 2D FEM code that is based on the unconditionally stable Newmark method. This effective stress-based formulation is based on the unconditionally stable generalized Newmark method that using the solid (displacement) - fluid (pore pressure) phase formulation (u-p) to solves the fully coupled Biot’s equations. This code has specialised constitutive models such as P-Z mark III model included in it that has been widely used to study the seismic behaviour of the structures and soil. Details of the u-p formulation and the functionality of this code can be found in (Zienkiewicz et al., 1999; Madabhushi and Zeng, 1998, 2006, 2007; Cilingir et al., 2011; Madabhushi and Madabhushi, 2015; Español-Espinel et al., 2023).

Dimensions of the model considered in the present analyses are shown in Figure 2. The 5 m span building is represented as a raft foundation located at a 0.5 m depth that applies a 50 kPa uniformly distributed surcharge. The rectangular tunnel is buried 7.5 m below the surface and horizontally 5 m from the footing edge. Tunnel lining and central dividing wall are modelled as 120 mm thick aluminium plates, which are equivalent to 300 mm thick concrete sections with equivalent bending stiffness. The EI and EA of the tunnel section in the prototype scale are $3.74 \times 106 \text{ MN/m}^2/\text{m}$ and $2.096 \times 105 \text{ MN/m}$, assuming the concrete stiffness as 25 GPa and the aluminium stiffness as 70 GPa. The static factor of safety against the tunnel flotation in saturated soil is a function of the soil overburden, tunnel structural self-weight, and buoyant force from the tunnel volume. For this tunnel section the FoS against floatation was determined to be 1.56. The numerical computation schedule includes two parts, i) static analysis to establish geo-static stresses in the soil and obtain the equilibrium of the tunnel-raft foundation system, ii) dynamic time-step analysis with the seismic loading applied as accelerations at the bedrock level. For the start of the dynamic analyses the geo-static stress state of the soil is obtained from the final stage of the static analysis. Four separate sets of analyses were carried out based on the same geometry shown in Figure 2. A sinusoidal wave with 10 cycles

of shaking was applied along the base bedrock nodes in all four sets of analyses. In case 1, the cut-and-cover tunnel was buried in dry soil without the building structure. Case 2 activated the adjacent building structure with the surcharge. Cases 3 and 4 were similar to cases 1 and 2, respectively, but with modified soil condition from fully dry to fully saturated.

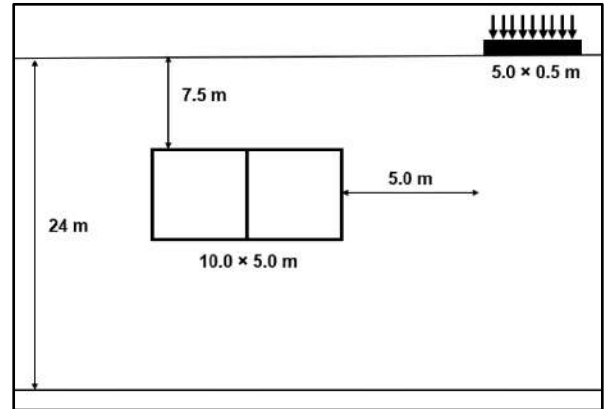


Figure 2 Dimension of the tunnel – footing system

2.1 Mesh Discretization

The finite element discretisation is conducted in three distinct zones, namely the loose sandy soil stratum, the rectangular tunnel transverse section, and the building foundation, as shown in Figure 3. All elements are quadrilateral with 8 solid nodes with 9 gauss points each, for capturing the displacements and accelerations at solid nodes and in-situ stresses and strains at the gauss points. For saturated analyses, each soil element has 4 additional fluid nodes overlain on corner solid nodes to create a fluid mesh to determine the pore pressures. In total, there are 452 elements with 3616 solid nodes and 1644 fluid nodes with 2 degrees of freedom for each solid node and 1 degree of freedom for each of the fluid nodes. The mesh size and the analysis domain need to be of reasonable size to keep the computational effort manageable. Following Semblat (2009) recommendations, the element size was chosen such that it is smaller than the 1/10th of the wavelength of the shear waves being transmitted. In these analyses the shear wave velocity was about 150 m/s and the main earthquake frequency is 1 Hz, so the wavelength is about 150 m. The element size of the largest element is about 2 m, which is $< 1/75$ th of the wavelength. So the shear waves would be transmitted without much distortion. During the saturated analysis, the water level is specified at the ground surface. Solid nodes along the bottom of the model are fully fixed in both horizontal and vertical directions. This enables the input motion to generate vertically propagated shear wave from the base of the model. The model side boundaries with the same y-coordinates are “tied” together, which means they experience the same displacement and acceleration. This boundary restraint works quite similar to the laminar model container used in centrifuge testing.

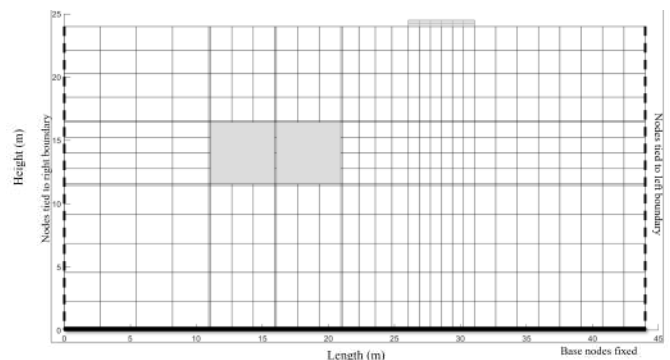


Figure 3 FE mesh discretization with applied boundary conditions

Table 1 Soil properties in the numerical analysis

Parameters	Value
Soil saturated density (kg/m ³)	1891
Void ratio	0.85
Poisson's ratio	0.3
Friction angle	33°
Dilatancy angle	3°
Cohesion (Pa)	100
Permeability (m/s)	1 × 10 ⁻⁴
Initial Young's modulus (MPa)	150
Initial bulk modulus (MPa)	50

2.2 Time Step Discretization

Dynamic analysis in the frequency domain is normally considered more cost-effective and less complicated. In this methodology, the input motion will be analysed separately as a group of sinusoidal components, and analysed modes are superposed to generate the final result. However, this methodology cannot capture the non-linear soil behaviour that is mobilised during the large shear strains imposed by the cyclic loading on the soil strata during an earthquake. The time domain analysis, although computationally more expensive, performs better in dynamic geotechnical problems by solving the model at each prescribed time step. The size of the elements and the time step controls the duration of the computation, as well as the accuracy of the outputs. This is particularly important when soil liquefaction is being considered in the boundary value problem.

Haigh et al. (2005) investigated the effect of different time steps in capturing the non-linear dynamic saturated soil behaviour. Significant differences were recorded in excess pore pressure and the acceleration time history with time steps of 1 ms, 5 ms, and 10 ms, which are two important parameters for understanding the dynamic responses. Research outputs recommended the error will be reduced to less than 5 % if there are more than 10-time steps being applied for the smallest discretised element. A decrease of the time step can cause considerable uncertainty in simulating the soil shear wave propagation, but excessive time step will significantly increase the computational time cost of the simulation. This study assumes the average soil shear wave velocity is about 150 m/s based on the initial soil bulk modulus and soil density, shown in Table 1. The smallest element in the model is the corner element of the tunnel lining with the dimension of 120 mm × 120 mm. The time step adopted in this study is 0.1 ms which means a total of 450,000-time steps are required for each analyses to achieve 45 s of simulation. This allows sufficient computational time step during the dynamic analysis, such that there are at least 10-time steps for the shear wave to propagate through the smallest soil elements.

2.3 Constitutive Models

As explained before, SWANDYNE analyses are carried out in two stages. First a static run is carried out to establish the geo-static stress state. The final stress state of this stage is used as the starting stress state for the dynamic analyses when the earthquake loading is applied. A modified Mohr-Coulomb model that is able to capture elastic-perfectly plastic soil behaviour was used for both the static and dynamic stages for the dry soil analyses (Chan, 1988). Soil constitutive models are considered separately in static and dynamic stages when dealing with saturated soil, as Mohr-Coulomb model is unable to capture excess pore pressure generation that occurs in this case. During the static analysis, a same modified Mohr-Coulomb type model as before was used. Details of key model parameters are given in Table 2. It should be noted that soil elastic and bulk modulus values given in Table 1 are implemented as the initial value to start the computation, the soil stiffness is modified during the analyses based on the soil strains, until the model reaches equilibrium. The analyses carried out in this research also specified the variation of the soil modulus with depth instead of a constant value to capture the realistic

soil modulus variations with effective confining pressure observed in the field.

Table 2 Parameters adopted in the Mohr-Coulomb Five model

Parameters	Value	Description
Work hardening modulus	100	
Switch to select yield Criterion	3	Mohr-Coulomb yield criterion
Switch to select soil modulus variation by depth	1	Specified by α
Reference mean confining pressure (kPa)	100	
Variation coefficient	$\alpha = 0.5$	Soil modulus varied with depth specified by square root

Table 3 Parameters adopted in the P-Z Mark III model

Parameters	Symbol	Value
Slope of the CSL for plastic potential	M_g	1.15
Slope of the CSL for yield surface	M_f	0.6
Dilatancy parameter for plastic potential	α_g	0.45
Dilatancy parameter for yield surface	α_f	0.45
Plastic modulus on loading (Pa)	$H_{loading}$	600
Plastic modulus on unloading (Pa)	$H_{unloading}$	4 × 10 ⁶
Permanent deformation parameter during unloading	γ_{Hu}	2
Permanent deformation parameter during reloading	γ_{DM}	0
Shear hardening parameter 1	β_0	4.2
Shear hardening parameter 2	β_1	0.2

The analyses carried out in this research also specified the variation of the soil modulus with depth instead of a constant value to capture the realistic soil modulus variations with effective confining pressure observed in the field. A generalized plasticity bounding surface model P-Z Mark III model (defined as DEP08F model in SWANDYNE, Chan (1988)), developed by Pastor et al. (1985), is implemented in the dynamic time step analysis. This model has been widely used by previous researchers (Chan, 1988; Madabhushi and Zeng, 1998; Haigh et al., 2005 etc.) in studying the dynamic saturated soil response. The P-Z Mark III model was used in these analyses as it is able to model the generation of excess pore pressures leading to liquefaction and consequent soil softening and the resulting plastic strains. This is in contrast to the Hardening model and hypoplastic model generally implemented into Plaxis that is widely used (Likitlersuang et al., 2014; Phutthananon et al., 2023; Muenpetch et al., 2023).

The P-Z Mark III model defines the plastic potential in eq (1), where the p' is the mean effective stress; q is the deviatoric stress; M_g is the slope of the critical state line (CSL), which is regarding the soil friction angle and Lode's angle.

$$G(p', q, p_g) = \{q - M_g p' \left(1 + \frac{1}{\alpha_g}\right) \left[1 - \left(\frac{p'}{p_g}\right)^{\alpha_g}\right]\} \quad (1)$$

The model yield surface is assumed to have the same shape as the plastic potential surface and therefore is defined similar to Equation (1). Parameters β_0 and β_1 are adopted to calculate the plastic modulus during the loading period, and the parameter γ_{Hu} is adopted to calculate the plastic modulus during the unloading period. Detail of model parameters is shown in Table 2 and have been fully explained by Zienkiewicz et al. (1998).

In this paper the same set of constitutive parameters were used in all the analyses and no fine tuning of individual parameters was carried out between the analyses.

3. DYNAMIC SOIL RESPONSE

3.1 Acceleration Time History

The dynamic analysis of the tunnel-soil-building system is conducted based on the final stage of the static simulation as explained before. The input ground motion during dynamic analysis is a sinusoidal motion with 10 cycles shaking and a peak ground acceleration (PGA) of around 0.2 g. This is a typical input motion obtained during the dynamic centrifuge tests carried out at Cambridge using the servo-hydraulic shaker (Madabhushi et al., 2012). The current boundary value problem was investigated under four different scenarios, varied by the soil moisture condition (dry or saturated) and the surface loading condition (with and without building surcharge).

Understanding the shear wave propagation is one of the key factors in investigating the dynamic soil response. Soil horizontal acceleration time histories in the free field are monitored from 5 m to the left side of the tunnel boundary. In Figure 4a, acceleration time histories in dry soil with corresponding Fast Fourier Transforms (FFTs) are presented, where $z = 0$ m at the surface, $z = 10$ m just below the tunnel invert, and $z = 20$ m at the bedrock level. In this figure, it can be seen that, as the horizontally polarised shear (Sh) waves propagate upwards towards the soil surface they amplify, with an amplification factor of 1.3 between the bedrock and the soil surface. However, the frequency content of the input motion remains unaltered at different depths. Further it can be seen that the presence of building on the other side of the tunnel has very little impact on these accelerations.

In Figure 4b, acceleration time histories in saturated soil and corresponding FFTs are presented. The same ground motion as the dry case was used as input at the base nodes of the model, and acceleration time histories are also outputted at the same locations. The soil response has reduced significantly after the first 2 cycles of shaking. This is an evidence that the soil is liquefied and therefore it is harder to transfer any shear waves once liquefaction has occurred. Wave propagation through saturated soil depends on the soil liquefaction ratio, which is relative to the residual soil effective stress. The maximum horizontal acceleration at $z = 20$ m is around 0.15 g (ignoring the first initial negative spike), which is approximately 70% of the input motion, this maximum horizontal acceleration dropped by 50 % at $z = 10$ m and $z = 5$ m and reach to almost 0% after the first 2 cycles.

Comparing Figure 4a and Figure 4b, it can be seen that the accumulation of excess pore pressures in the soil medium plays a significant role in effecting the propagating shear waves. The excess pore pressure build-up is discussed in the next section separately. In addition, the presence of the surface surcharge did not make a significant influence on the acceleration time history in both dry and saturated scenarios. This is to be expected as the vertical array of output stations were reasonably far from the surcharge location and the tunnel location, that this can be considered as a “free-field” response.

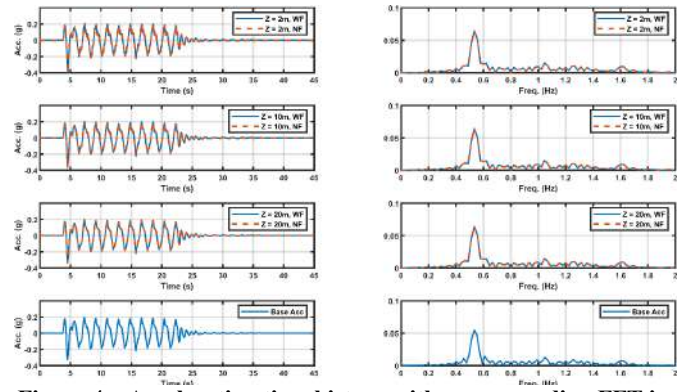


Figure 4a Acceleration time history with corresponding FFT in the dry soil

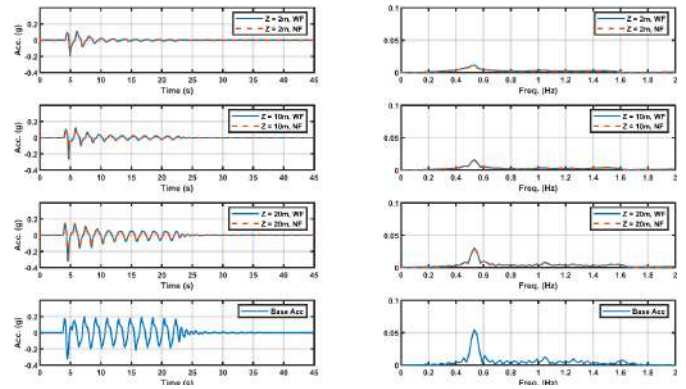


Figure 4b Acceleration time history with corresponding FFT in the saturated soil

3.2 Excess Pore Pressure

Based on the classical soil effective stress principle by Terzaghi (1943), liquefaction can be defined as the reduction of the effective stress caused by the generation of excess pore pressures (over and above the hydrostatic pore pressures). Excess pore pressures are generated due to the tendency of soil to undergo volumetric contraction due to shear stresses under cyclic loading. Excess pore pressures at depths of 2 m, 10 m, and 20 m below the surface are monitored to study the liquefaction ratio. In addition, the excess pore pressure contours are also shown in Figure 5a and Figure 5b at the time instant of 10 s to give an overview of the spatial distribution of the liquefaction ratio.

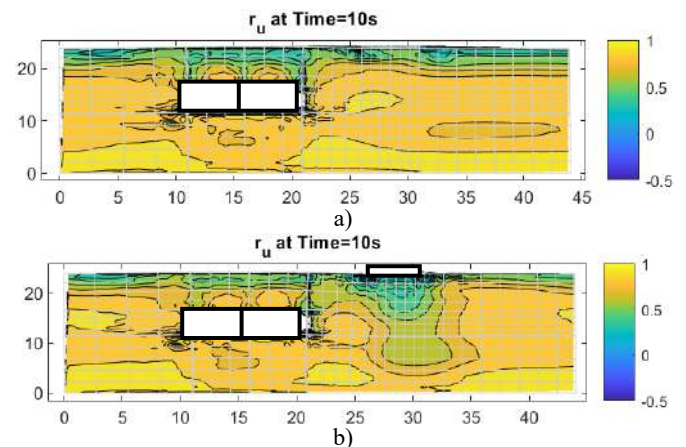


Figure 5 Liquefaction ratio contour for the analyses a) without the structure; b) with the structure

In these figures, it can be seen that widespread liquefaction has occurred in both cases by 10 s especially at soil depths below the tunnel. At the shallow depths of $z < 2$ m, the liquefaction ratio is about 0.5 at this time, probably due to the proximity of the soil surface and shorter drainage distance.

Excess pore pressure time histories at the far-field and mid-field are presented in Figures 6a and 6b, respectively. The accumulation of excess pore pressures is captured satisfactorily along the entire input motion. The soil at the depths of 10 m and 20 m is fully liquefied at both far-field and mid-field, as the excess pore pressure are about equal to the static effective stress. The presence of the surface building causes a significant difference in the excess pore pressure at shallow depth. Additional vertical load from the building foundation led to the monotonic shearing movement of the upper layer of soil as the building settles, inducing further dilatant behaviour from the soil. This manifests as a quick drop in the excess pore pressure, which is shown in Figure 6b at $z = 2$ m. However, this phenomenon becomes less obvious for the deeper soil due to the reduction in the effect of surface surcharge with depth.

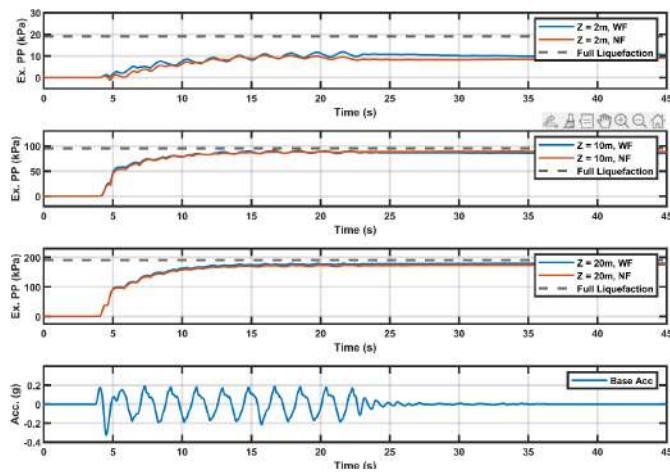


Figure 6a Excess pore pressure time history in the far-field

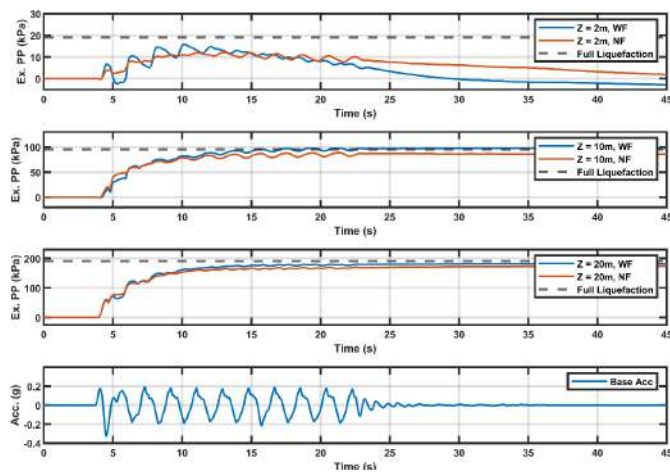


Figure 6b Excess pore pressure time history in the near field (between tunnel and footing)

The uplift of the tunnel, and the accumulation of the excess pore pressure below the tunnel invert recorded during the sinusoidal earthquake are presented in Figure 7 along with the input motion. In this figure, the uplift suffered by the tunnel is around 1 m, which is consistent with the peak surface heave shown in Figure 8. This suggests that the soil above the tunnel crown has developed compressive axial strain when the tunnel was uplifting. The presence of the adjacent structures did not significantly affect the tunnel uplift or the excess pore pressure generation below the tunnel. This may not be the case if the surface structure is much closer to the tunnel. The soil below the tunnel liquefied after around 2 cycles of the shaking.

The soil liquefaction ratio then started to decrease due to the suction around the tunnel invert, caused by the tunnel uplift.

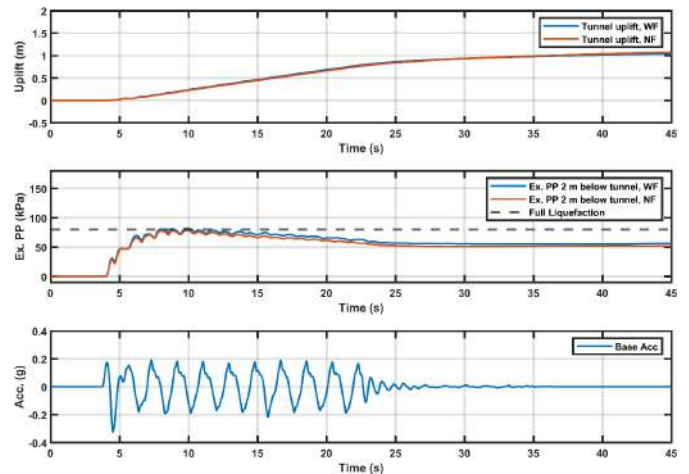


Figure 7 Uplift and excess pore pressure generation of the tunnel during the sinusoidal earthquake

3.4 Soil Deformations

Soil surface vertical displacement profiles during and after shaking are shown in Figure 8, where NF represents the modelling case without building surcharge and foundation and WF represents the modelling case with building surcharge and foundation. Soil movements are observed at different times along the input motion. Time point 1 presents the soil profile after 2 cycles of shaking and time point 2 presents the soil profile in the post-shaking stage. In saturated cases, the tunnel tends to uplift during the earthquake due to its buoyancy.

The total soil volume largely remains constant within the time scale of the input motion, due to the relatively undrained soil state. The magnitude of soil uplift was enhanced due to the accumulation of the excess pore pressure, with a peak upward displacement of around 1 m. This uplift limit seems to be not affected by the existence of the additional surface surcharge. However, the building suffered additional settlement due to rapid degradation in the soil stiffness due to liquefaction. The foundation experienced approximately 10° clockwise rotation, which can lead to serious safety risks if a multi-storey building is constructed on such foundations. In contrast, the surface displacement and building rotation are comparatively neglectable in dry soil. Furthermore, relatively obvious displacements are observed near the model side boundaries due to the horizontal soil inertia force.

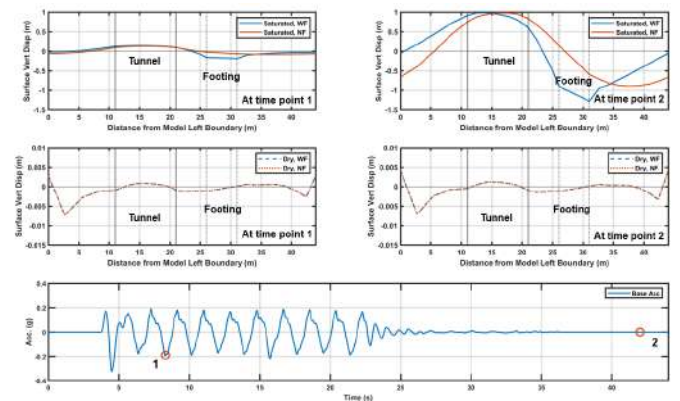


Figure 8 Soil surface displacement profiles with the input motion

The soil displacement vectors under saturated soil without and with footing are presented in Figures 9a and 9b, respectively. The cover soil above the tunnel crown has been pushed upward due to the tunnel flotation. In addition, the soil at the bottom tends to fill the

“gap” below the tunnel invert, which is presented by circular loops on both sides of the tunnel. Similar soil movements have also been observed from the 1-g shaking table testing by Watanabe et al. (2016), and the dynamic centrifuge testing by Chian et al. (2014), the latter for circular tunnels. In addition, the existence of the building foundation with surcharge causes unbalanced soil movements along the surface. This enhances the soil uplift on the left side of the tunnel. Further, the lateral boundary movements are consistent at any given depth due to the tided boundary condition.

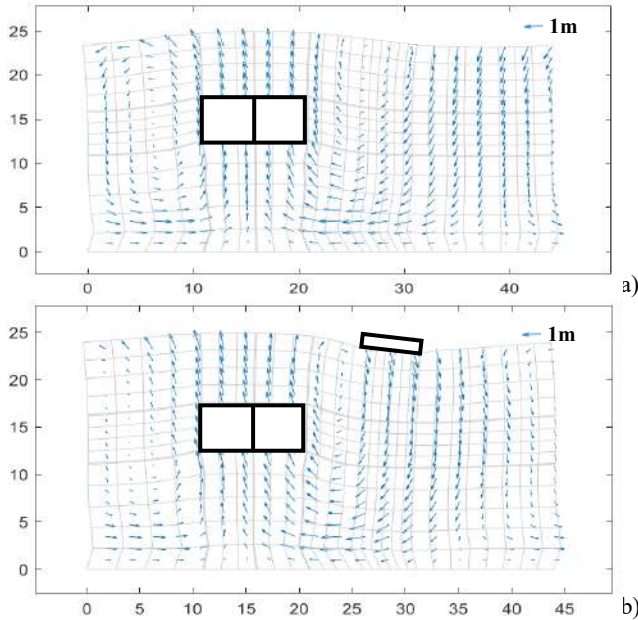


Figure 9 Traces of soil displacements in the saturated soil (magnification factor of 1), a) without footing; b) with footing

3.5 Soil Earth Pressure

Earth pressures are obtained from adjacent soil elements along the tunnel lining. Vertical effective stresses are recorded during the numerical analyses at the tunnel crown and invert, and horizontal effective stresses are recorded for tunnel sidewalls. Figures 10a and 10b show numerical results of the soil earth pressure distribution along the tunnel lining under dry soil, without and with the building surcharge respectively. Dynamic earth pressures are analysed by comparing observations in 4 different stages, namely the static stage, after 2 cycles and 4 cycles of shaking, and the post-shaking stage. Lateral soil pressures along tunnel sidewalls are also compared with analytical interpretations by implementing the at-rest earth pressure coefficient K_0 , Rankine’s earth pressure coefficients K_a , K_p , and Mononobe-Okabe’s dynamic earth pressure coefficients K_{AE} , K_{PE} .

Soil vertical stress along the tunnel crown shows some variation during the static analysis, owing to the tunnel lining flexibility. During the seismic loading, the variations in the vertical stress are rather small. This may be due to the constant overburden stress acting on the crown of the wall. However, the residual vertical stress is quite different to the pre-shaking stresses. Similarly, the earth pressure applied on the tunnel invert is about the sum of the weight of covered soils plus the structural weight of tunnel lining. Significant stress concentrations are observed on both edges of the tunnel crown and invert. Moreover, dynamic lateral response along tunnel sidewalls is much more complicated. Earth pressures were also obtained during the input motion (after 2 cycles or 4 cycles of shaking) and in post-seismic residual period. In addition, the middle of side walls experiences a dip in the horizontal stresses owing to the inward deformation of the tunnel lining. The presence of the building foundation with structural load introduces an additional lateral earth pressure on the righthand side wall of the tunnel as seen in Figure 10b. This increase lateral earth pressure occurs towards to the top of this wall which is the closest region to the raft foundation.

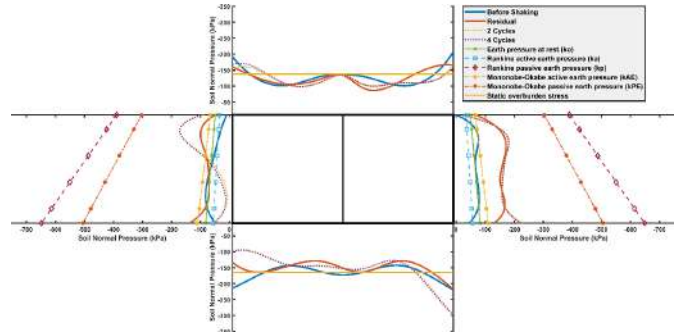


Figure 10a Soil earth pressure distribution under dry soil without footing

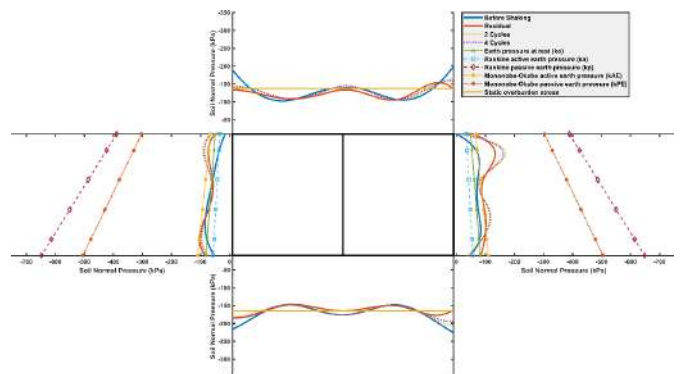


Figure 10b Soil earth pressure distribution under dry soil with footing

Figures 11a and 11b present the dynamic response under saturated condition without and with footing respectively. Initial earth pressures acting on the tunnel crown are approximately equal to soil effective vertical stresses, which are greater than earth pressures applied on the tunnel invert due to the buoyancy of the tunnel. During the earthquake, soil earth pressures dropped significantly to near zero values. This is because the soil surrounding the tunnel is liquefied due to significant excess pore pressure generation. The presence of the building foundation with surcharge provides an unchanged vertical effective stress, which causes obvious stress concentration on the right edge of the tunnel invert, shown in Figure 11b. Moreover, it is possible that the liquefaction ratio for the soil in the tunnel-building interaction zone is significantly different from the soils in the free field. This can also be inferred by the non-uniform settlement within the footing, shown in Figure 8 and consequent rotation of the footing. Dynamic lateral responses along tunnel sidewalls were also attenuated, following the maximum sidewall earth pressure obtained after 4 cycles of shaking. In addition, it seems that the existence of the building surcharge mitigates the residual stress concentration at the bottom edge of the right-side wall.

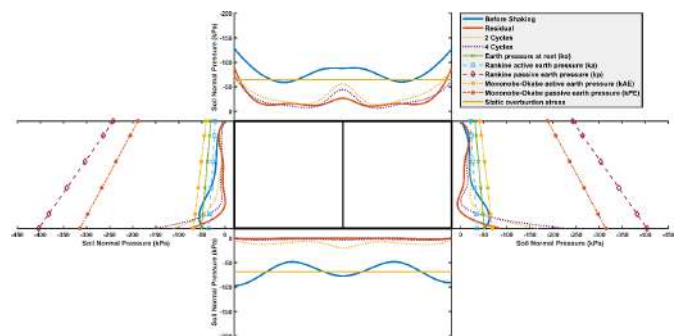


Figure 11a Soil earth pressure distribution under saturated soil without footing

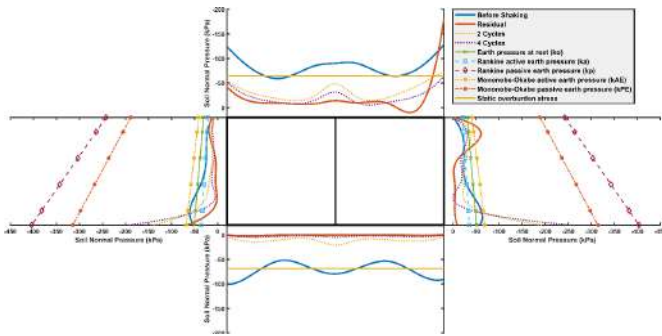


Figure 11b Soil earth pressure distribution under saturated soil with footing

In summary, dynamic earth pressures around the tunnel lining are investigated in different soil moisture and surface loading conditions. Tunnel crown and invert lining experienced significant vertical stress reduction in the fully saturated condition, due to the liquefaction of adjacent soils. The vertical stress distribution along the same lining location is relatively more stable in the fully dry soil. Tunnel sidewalls observed the stress concentration at the corner of the lining in the saturated condition. Earthquake induced liquefaction changed the physical behaviour of the saturated soil that residual lateral earth pressures are smaller than Rankine’s and Mononobe-Okabe’s active earth pressure lines. The presence of the building foundation caused imbalance in the overburden stress above the tunnel crown. This enhances the stress concentration at the top right corner of the tunnel lining in the saturated soil.

4. DYNAMIC TUNNEL RESPONSE

The bending moment for tunnel lining elements under the input motion is predicted by adopting the beam flexural formula and knowing the appropriate vertical or horizontal stresses at the gauss points of the elements. Each of the elements in this model has 9 gauss points with equal spacing. The location of each gauss point on a square element is shown in Figure 12. The element bending stress is determined as the difference of axial stresses between 2 central gauss points, that is vertical stresses of gauss points 4 and 6 for the left and right sidewalls, and horizontal stresses of gauss point 2 and 8 for the tunnel crown and invert. The distance to the neutral axis is equal to the spacing between 2 gauss points, which is approximately equal to 80% of the element length.

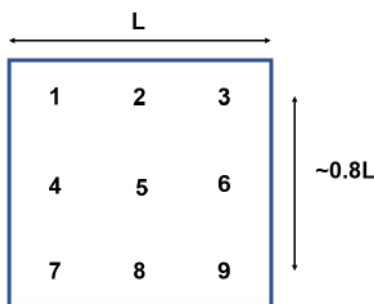


Figure 12 Gauss points locations on a square element

Tunnel bending moment diagrams without and with building foundation, during the input motion under dry soil are shown in Figure 13a and Figure 13b. The tunnel bending moment did not vary significantly after 2 cycles and 4 cycles of shaking, compared with the initial and residual magnitudes. Bending stresses are concentrated near the connection between the middle dividing wall and tunnel crown lining. The connection between the dividing wall and tunnel invert lining experienced less stress concentration comparing with the connection with tunnel crown lining, and the maximum bending

moment occur at two corners. Peak values along both sidewalls are recorded just above the corner between the tunnel sidewall and invert, which are approximately 3.5 times greater than the bending moments at the middle of the sidewall. The presence of the building foundation with surcharge contributes very little to the tunnel structural response, unlike the horizontal earth pressures seen earlier.

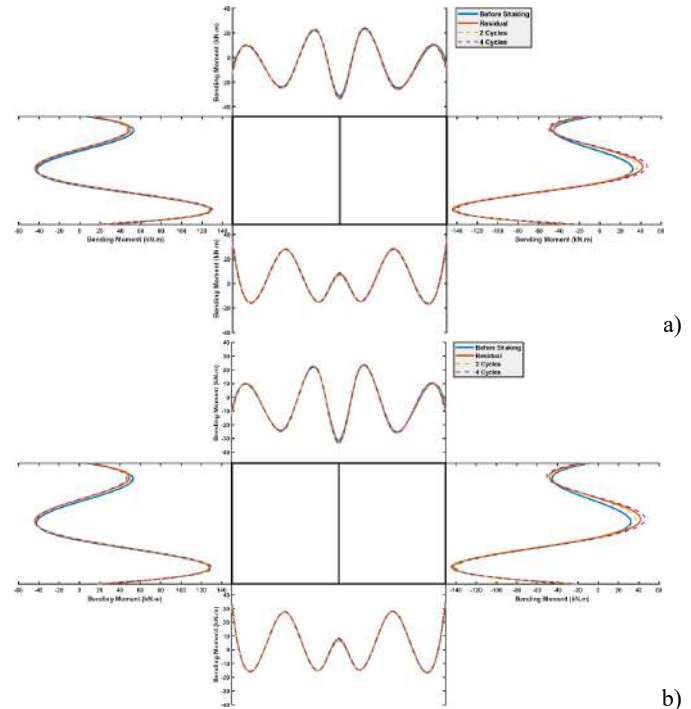


Figure 13 Tunnel lining bending moment distribution under dry soil a) without footing; b) with footing

Figures 14a and 14b show the envelope of the tunnel lining bending moments under saturated soil without and with the building surcharge. Tunnel crown lining experiences significantly larger bending moments without the presence of the building foundation. Peak bending moments occur at the connection of the dividing wall at the middle of two underground openings. The magnitude of the bending moment is decreased from about 150 kNm to 20 kNm in presence of the building surcharge. Similar observation is recorded at the tunnel invert lining, that residual bending moments are decreased from 50 kNm to about 5 kNm at the connection between the dividend wall and tunnel invert, and from 160 kNm to about 40 kNm at the middle of the two underground openings. The residual bending moments are doubled at the middle of the sidewall after shaking. In addition, the maximum bending moments along the tunnel sidewall occurred just above the bottom corner of the tunnel invert, increased from about 140 kNm to 220 kNm due to the accumulation of the pore pressure.

Furthermore, the maximum bending stresses along the tunnel lining are observed during the input motion (after the first 2 cycles or 4 cycles) than in the post-shaking period. This may be explained by the significant inertial force generated from the saturated sand acting on the tunnel sidewall. In summary, the dynamic tunnel response is highly sensitive when the soil is saturated and excess pore pressure generation occurs during the cyclic loading, and the effect of the building interaction is mostly on the tunnel crown.

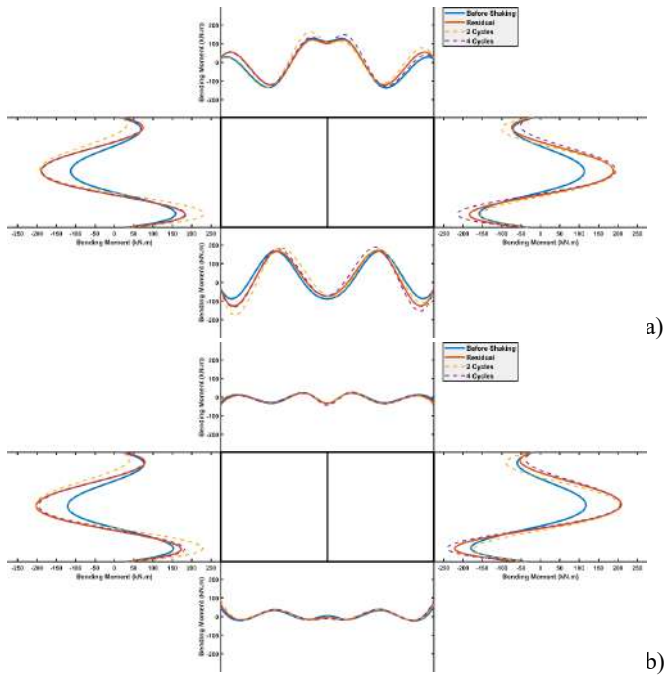


Figure 14 Tunnel lining bending moment distribution under saturated soil a) without footing; b) with footing

5. CONCLUSIONS

Considering the interaction between the surface and sub-surface structures is necessary for correct understanding the dynamic tunnel behaviour. In this study, a set of dynamic finite element models were simulated using SWANDYNE code to investigate four different scenarios. Soil surface displacement, earth pressure, wave propagation and tunnel structural response were all investigated. Two types of soil moisture conditions are considered: firstly, the fully saturated case and secondly the fully dry case. The building foundation with surcharge is initially deactivated in the model as a reference scenario to investigate the effect of tunnel – building interaction. The earthquake input motion considered was a sinusoidal wave with 10 cycles of shaking and PGA of about 0.2 g.

In saturated cases, the soil acceleration along various depths attenuated dramatically after first 2 cycles of shaking due to the occurrence of liquefaction. The liquefaction ratio depends on the generation of excess pore pressures and the magnitude of residual effective stresses. The tunnel flotation following the uplift of overburden soil is a key seismic design consideration, in particular for shallow underground tunnels constructed using cut-and-cover method in saturated soil. The existence of building surcharge mitigates the soil liquefaction in sub-surface within the interaction zone between the tunnel and footing. In addition, tunnel lining structural responses along the crown and invert observed significant differences in the presence of the building surcharge. This highlights the importance of considering a variety of surface structure interactions with tunnels.

In the dry case, the soil surface movement becomes negligible. Wave propagation through the soil is also not affected by the surface structure interaction at different depths. The bending moment distribution along the tunnel lining remains stable and largely unchanged during the input motion. The maximum earth pressure and tunnel bending moment are increased during the input motion compared to the post-shaking period, in both saturated and dry cases.

This numerical study shows the significant effect of the soil liquefaction induced excess pore pressure generation on the large soil plastic deformation and tunnel lining structural response. This is a distinct difference with the same tunnel-building system but under the dry sand. It is possible to model the soil liquefaction with other constitutive models such as Sanisand (Dafalias and Manzari, 2004) or PM4Sand (Boulanger and Ziotopoulou, 2013). Further research is recommended using different constitutive models so that more

detailed analysis of the excess pore pressure around the tunnel lining can be investigated.

A series of dynamic Geotechnical centrifuge tests are scheduled by adopting the Turner beam centrifuge with a rotational radius of 4.125 m at the Schofield Centre, Cambridge University. The proposed centrifuge testing data will be used to calibrate the numerically simulated dynamic tunnel and soil responses.

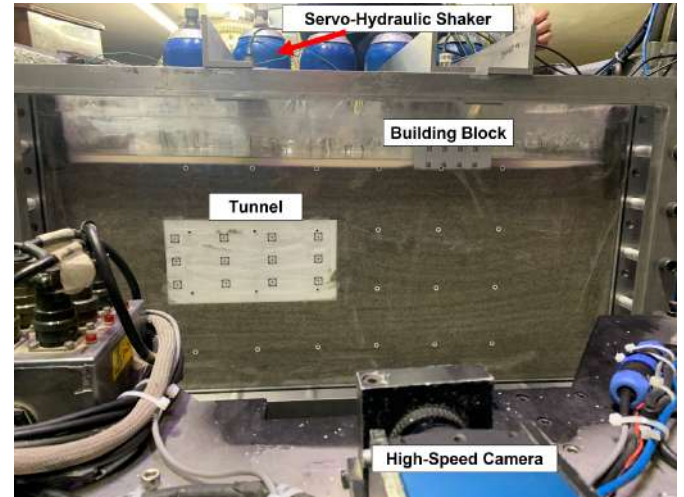


Figure 15 Prepared centrifuge model in saturated loose sand on 31st Jan 2023

6. ACKNOWLEDGMENTS

The authors would like to appreciate to the technicians at the Schofield Centre. Additionally, the first author sincerely appreciates Prof. Gopal Madabhushi for his constant support during this toughest period of the recent death of the first author's grandparents.

7. REFERENCES

- Bilotta, E., Lanzano, G., Madabhushi, S. P., & Silvestri, F. (2014). "A Numerical Round Robin on Tunnels under Seismic Actions." *Acta Geotechnica*, 9(4), 563-579. doi:10.1007/s11440-014-0330-3.
- Bilotta, E., Paolillo, A., Russo, G., & Aversa, S. (2017). "Displacements Induced by Tunnelling under a Historical Building." *Tunnelling and Underground Space Technology*, 61, 221-232. doi:10.1016/j.tust.2016.10.007.
- Boulanger, R. W., & Ziotopoulou, K. (2013). "Formulation of a Sand Plasticity Plane-Strain Model for Earthquake Engineering Applications." *Soil Dynamics and Earthquake Engineering*, 53, 254-267. doi: 10.1016/j.soildyn.2013.07.006.
- Chan, A. H. C. (1988). "A Unified Finite Element Solution to Static and Dynamic Problems of Geomechanics." (*Doctoral dissertation, Swansea University*).
- Chian, S. C., & Madabhushi, S. P. G. (2012). "Effect of Buried Depth and Diameter on Uplift of Underground Structures in Liquefied Soils." *Soil Dynamics and Earthquake Engineering*, 41, 181-190. doi:10.1016/j.soildyn.2012.05.020.
- Chian, S. C., Tokimatsu, K., & Madabhushi, G. (2014). "Soil Liquefaction-Induced Uplift of Underground Structures: Physical and Numerical Modeling." doi:10.1061/(asce)gt.1943-5606.0001159.
- Chou, J. C., Kutter, B. L., Travasarou, T., & Chacko, J. M. (2011). "Centrifuge Modeling of Seismically Induced Uplift for the BART Transbay Tube." *Journal of Geotechnical and Geoenvironmental Engineering*, 137(8), 754-765. doi: 10.1061/(asce)gt.1943-5606.0000489
- Chou, J. C., Kutter, B., and Travasarou, T. (2008a). "Centrifuge Testing of the Seismic Performance of a Submerged Cut-and-Cover Tunnel in Liquefiable Soil Centrifuge Data Report for Test Series JCC01." *Network for Earthquake Engineering Simulation*

- (NEES) Program, Center of Geotechnical Modeling, Univ. of California, Davis, CA.
- Chou, J. C., Kutter, B., and Travarasrou, T. (2008b). "Centrifuge Testing of the Seismic Performance of a Submerged Cut-and-Cover Tunnel in Liquefiable Soil Centrifuge Data Report for Test Series JCC02." *Network for Earthquake Engineering Simulation (NEES) Program, Center of Geotechnical Modeling, Univ. of California, Davis, CA.*
- Cilingir, U., & Madabhushi, S. G. (2011a). "Effect of Depth on the Seismic Response of Square Tunnels." *Soils and Foundations*, 51(3), 449-457. doi: 10.3208/sandf.51.449.
- Cilingir, U., & Madabhushi, S. G. (2011b). "A Model Study on the Effects of Input Motion on the Seismic Behaviour of Tunnels." *Soil Dynamics and Earthquake Engineering*, 31(3), 452-462. doi: 10.1016/j.soildyn.2010.10.004.
- Cilingir, U., & Madabhushi, S. G. (2011c). "Effect of Depth on Seismic Response of Circular Tunnels." *Canadian Geotechnical Journal*, 48(1), 117-127. doi: 10.1139/t10-047.
- Cilingir, U., Haigh, S. K., Madabhushi, S. P. G., & Zeng, X. (2011). "Seismic Behaviour of Anchored Quay Walls with Dry Backfill." *Geomechanics and Geoengineering*, 6(3), 227-235. doi:10.1080/17486025.2011.578670.
- Dafalias, Y. F., & Manzari, M. T. (2004). "Simple Plasticity Sand Model Accounting for Fabric Change Effects." *Journal of Engineering Mechanics*, 130(6), 622-634. doi: 10.1061/(asce)0733-9399(2004)130:6(622).
- Español-Espinel, C., Haigh, S. K., & Madabhushi, G. S. (2023). "Liquefaction Analysis of Soil Plugs within Large Diameter Monopiles using Numerical Modelling." *Bulletin of Earthquake Engineering*, 21(12), 5443-5458. doi: 10.1007/s10518-023-01742-7.
- Haigh, S. K., Ghosh, B., & Madabhushi, S. P. (2005). "Importance of Time Step Discretisation for Nonlinear Dynamic Finite Element Analysis." *Canadian Geotechnical Journal*, 42(3), 957-963. doi: 10.1139/t05-022.
- Hong-in, P., Keawsawasvong, S., Lai, V. Q., Nguyen, T. S., Tanapalungkorn, W., & Likitlersuang, S. (2023). "3D Stability and Failure Mechanism of Undrained Clay Slopes Subjected to Seismic Load." *Geotechnical and Geological Engineering*, 1-29. doi:10.1007/s10706-023-02497-3.
- Lanzano, G., Bilotta, E., Russo, G., Silvestri, F., & Madabhushi, S. G. (2012). "Centrifuge Modeling of Seismic Loading on Tunnels in Sand." *Geotechnical Testing Journal*, 35(6), 854-869. doi: 10.1520/gtj104348.
- Likitlersuang, S., Surarak, C., Suwansawat, S., Wanatowski, D., Oh, E., & Balasubramaniam, A. (2014). "Simplified Finite-Element Modelling for Tunnelling-Induced Settlements." *Geotechnical Research*, 1(4), 133-152. doi:10.1680/gr.14.00016.
- Madabhushi, S. P. G., & Zeng, X. (1998). "Seismic Response of Gravity Quay Walls. II: Numerical Modeling." *Journal of Geotechnical and Geoenvironmental Engineering*, 124(5), 418-427. doi:10.1061/(asce)1090-0241(1998)124:5(418).
- Madabhushi, S. P. G., & Zeng, X. (2006). "Seismic Response of Flexible Cantilever Retaining Walls with Dry Backfill." *Geomechanics and Geoengineering: An International Journal*, 1(4), 275-289. doi:10.1080/17486020601039170.
- Madabhushi, S. P. G., & Zeng, X. (2007). "Simulating Seismic Response of Cantilever Retaining Walls." *Journal of Geotechnical and Geoenvironmental Engineering*, 133(5), 539-549. doi:10.1061/(asce)1090-0241(2007)133:5(539).
- Madabhushi, S. S. C., & Madabhushi, S. P. G. (2015). "Finite Element Analysis of Floatation of Rectangular Tunnels Following Earthquake Induced Liquefaction." *Indian Geotechnical Journal*, 45(3), 233-242. doi:10.1007/s40098-014-0133-3.
- Mase, L. Z., Tanapalungkorn, W., Likitlersuang, S., Ueda, K., & Tobita, T. (2022). "Liquefaction Analysis of Izumio Sands under Variation of Ground Motions during Strong Earthquake in Osaka, Japan." *Soils and Foundations*, 62(5), 101218. doi:10.1016/j.sandf.2022.101218.
- Miranda, G., Nappa, V., Bilotta, E., Haigh, S. K., & Madabhushi, G. S. (2023). "Physical Modelling of the Interaction between a Tunnel and a Building in a Liquefying Ground and its Mitigation." *Tunnelling and Underground Space Technology*, 137, 105108. doi:10.1016/j.tust.2023.105108.
- Muenpetch, N., Keawsawasvong, S., Komolvilas, V., & Likitlersuang, S. (2023). "Numerical Investigation on Impact of Excavations in Influence Zone of Existing MRT Tunnels." *Geomechanics and Geoengineering*, 1-20. doi:10.1080/17486025.2023.2226107.
- Paston, M., Zienkiewicz, O. C., & Leung, K. H. (1985). "Simple Model for Transient Soil Loading in Earthquake Analysis. II. Non-Associative Models for Sands." *Intl J for Num & Analytical Methods in Geomechanic*, 9(5). doi:10.1002/nag.1610090506.
- Petchkaew, P., Keawsawasvong, S., Tanapalungkorn, W., & Likitlersuang, S. (2023). "Seismic Stability of Unsupported Vertical Circular Excavations in c-φ Soil." *Transportation Infrastructure Geotechnology*, 10(2), 165-179. doi:10.1007/s40515-021-00221-3.
- Petchkaew, P., Keawsawasvong, S., Tanapalungkorn, W., & Likitlersuang, S. (2023). "3D Stability Analysis of Unsupported Rectangular Excavation under Pseudo-Static Seismic Body Force." *Geomechanics and Geoengineering*, 18(3), 175-192. doi:10.1080/17486025.2021.2019321.
- Phutthananon, C., Lertkultanon, S., Jongpradist, P., Duangsano, O., Likitlersuang, S., & Jamsawang, P. (2023). "Numerical Investigation on the Responses of Existing Single Piles due to Adjacent Twin Tunneling Considering the Lagging Distance." *Underground Space*, 11, 171-188. doi:10.1016/j.undsp.2022.12.005.
- Semblat, J. F., & Brioist, J. J. (2009). "Efficiency of Higher Order Finite Elements for the Analysis of Seismic Wave Propagation." *Journal of Sound and Vibration*, 231(2), 460-467. doi:10.1006/jsvi.1999.2636.
- Sukkarak, R., Tanapalungkorn, W., Likitlersuang, S., & Ueda, K. (2021). "Liquefaction Analysis of Sandy Soil during Strong Earthquake in Northern Thailand." *Soils and Foundations*, 61(5), 1302-1318. doi:10.1016/j.sandf.2021.07.003.
- Taylor, E. J., & Madabhushi, S. P. G. (2020). "Remediation of Liquefaction-Induced Floatation of Non-Circular Tunnels." *Tunnelling and Underground Space Technology*, 98, 103301. doi: 10.1016/j.tust.2020.103301.
- Terzaghi, K. (1943). "Theoretical Soil Mechanics." *John Wiley and Sons Inc., New York*, 314.
- Tsinidis, G., de Silva, F., Anastasopoulos, I., Bilotta, E., Bobet, A., Hashash, Y. M., ... & Fuentes, R. (2020). "Seismic Behaviour of Tunnels: From Experiments to Analysis." *Tunnelling and Underground Space Technology*, 99, 103334. doi: 10.1016/j.tust.2020.103334.
- Watanabe, K., Sawada, R., & Koseki, J. (2016). "Uplift Mechanism of Open-Cut Tunnel in Liquefied Ground and Simplified Method to Evaluate the Stability against Uplifting." *Soils and Foundations*, 56(3), 412-426. doi: 10.1016/j.sandf.2016.04.008.
- Zienkiewicz, O.C., Chan, A.H.C., Pastor, M., Schrefler, B.A., & Shiomi, T. (1998). "Computational Geomechanics with Special Reference to Earthquake Engineering." *John Wiley & Sons, New York*. doi:10.1002/1099-1484(200011)5:8<673::aidcfm112>3.3.co;2-x.
- Zienkiewicz, O. C. (1999). *Computational Geomechanics with Special Reference to Earthquake Engineering*. John Wiley. ISBN: 978-0-471-98285-2